The 2013 World Congress on
Advances in Nano, Biomechanics, Robotics, and Energy Research (ANBRE13)
Seoul, Korea, August 25-28, 2013

Investigation of passive air cooling capacity for spent fuel pool

Po-Chih Tsao[1)], Kai-Ting Hsieh[2)], Duen-Sheng Lee[3)],
Chang Nyung Kim[4)], Yung-Shin Tseng[5)] and *Tzu-Chen Hung[6)]

[1)] *Institute of Mechatronic Engineering,*
National Taipei University of Technology (NTUT), Taiwan
[2)] *Graduate Institute of Mechanical and Electrical Engineering, NTUT, Taiwan*
[3)] *Department of Mechanical Engineering, Kyung Hee University, Korea*
[4)] *Department of Engineering and System Science,*
National Tsing Hua University, Taiwan
[5)] *Department of Mechanical Engineering, NTUT, Taiwan*
**Tel: +886-2-2771-2171#2021; tchung@ntut.edu.tw*

ABSTRACT

This study proposes to upgrade the security of spent fuel pool (SFP) by passive heat transfer. In case SFP is waterless after accident, air is the only medium to remove the heat out of the pool. The flow phenomena will be investigated via mainly computational fluid dynamics (CFD) and the auxiliary of experiments. The internal and viscous resistances of air flow in the fuel assemblies are important parameters when the technique of porous media, which can tremendously reduce the amount of numerical meshes, is employed. For the reliability of the research, this study also sets up experiment equipment to verify the CFD simulation. This study has investigated to find out the important parameters to improve the design of the SFP. Results of experiments and simulations have indicated that the arrangement of opening and height of backplane significantly influence the temperature distribution in the SFP (about 10% to 20%). In addition, arrangement of fuel bundles and the gap of air channel are also important factors.

Keywords: Spent fuel pool (SFP); passive heat transfer; CFD

1. INTRODUCTION

The Fukushima Daiichi nuclear disaster caused the loss of adequate cooling capability to spent fuel pool and the releases of radioactive materials (ANS 2012). Accordingly, the safety of spent fuels has been in the spot issue among all the concerns, and it's important to assure safety removing the decay heat of spent fuels completely. Spent fuel rods discharged from the reactors have massive decay heat (Bodansky 2000), and stored in wet-storage pools or dry-storage casks in practice (Iqbal *et al*. 2006). Compared with dry storage, wet storage has the advantage of removing decay heat and providing a barrier for any releases of radioactive (e.g., Biro

[1), 2), 3)] Graduate Student
[4), 5), 6)] Professor

and Rodna 2003, Arndt *et al*. 2003, Steinberg and Afanasyev 2003). For a dry-storage system, it's only suitable for lower-rate of decay heat spent fuel (U.S. NRC 1997).However, after accident, SFP is waterless soon, and air is the only medium to remove the heat from the pool. Therefore, it's necessary to take measures to upgrade the security of spent fuel pool (SFP) by a passive cooling design. This investigation was made mainly to find out the important parameters for the design.

Navarro *et al*. (2011) used the k-ε model that presents results of flow simulations performed with the CFD code in a PWR 5 × 5 rod bundle segment with a split-vane spacer grid. Smith *et al*. (2002) compared several test results with CFD predictions in a 5 x 5 rod bundle with the mixing vane spacer grid using the renormalization group (RNG) *k-ε* model, and proved the validity of CFD as a tool to investigate flow and temperature distributions in a PWR fuel bundle. Besides, Conner *et al*. (2010) presented a specific 5 × 5 rod bundle CFD model and showed how the results of CFD simulation match the test data, thus validating the CFD methodology. For this study, we will also use the *k-ε* model in a 5 × 5 rod bundle. Since Hung *et al*. (2013) have successfully simulated the thermal-hydraulic behavior of the spent-fuel pool using the technique of porous-medium to simplify the analysis. In this research, we will use this method to reduce the amount of numerical meshes. Niyogi and Tseng (1983) illustrate, with examples, the design of effective cooling systems for spent fuel pools, following various operational with thermal-hydraulic, and that give us lots of revelations about the parameters.

In order to find out the important parameters to improve the design of the SFP, CFD is employed to investigate the air cooling capacity of the spent fuel pool in this study. Meanwhile, experiment will been set up to verity the CFD simulation.

2. A PASSIVE AIR COOLING EXPERIMENTAL SFP MODEL

2.1 Experiment's equipment

As shown in Fig. 1, the equipment of the experiment is mainly a combination of aluminum extrusion, tempered glass and five assemblies of heaters. In the present study, only 5 bundles are installed. The concept of passive heat transfer is

Fig. 1 Experimental equipment

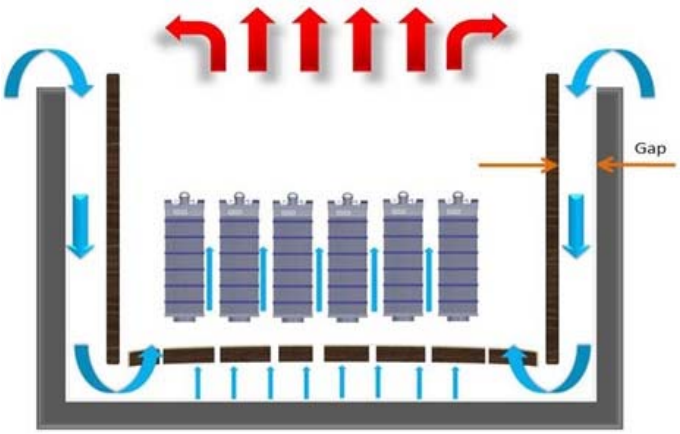

Fig. 2 Passive heat transfer concept diagram

demonstrated in Fig. 2. Due to temperature caused density difference along the fuels, buoyancy force drives air flowing from the external channel, the bottom of fuel bundles to the outflow of the internal tank.

2.2 Measurement installation

As shown in Fig. 3, the measurement tools include k-type thermal couple, wind gauge, current transformer, variable resistor, silicon-controlled rectifier (SCR) and data logger. The thermal couple was installed at the height of 10 cm and 70 cm on a rod and every rod located at the center of a bundle will have an additional thermal couple at 40 cm. In this paper, the input powers are 1000 W, 3000 W and 4000 W, and they can by adjusted by the variable resistor.

Fig. 3 Thermal couple, wind gauge, variable resistor and current transformer

2.3 Passive heat transfer experiment

The purpose of this study is mainly to compare the temperature distribution of different parameters. The parameters include the openings arrangement of backplane, the height of the backplane, forced convection, width of inlet air channel, etc. This paper mainly explores the effect of power of rod bundles, openings arrangement and height of backplanes. Three openings arrangements for the backplane are as shown in

Fig. 4. From left to right, the first arrangement has only one row of square holes for rod bundles open (Case 1). The second arrangement has all the round holes and three rows of square holes for rod bundles open (Case 2). The third has all the round holes and one row of square holes for rod bundles open (Case 3). Height of the backplane, as shown in Fig. 5 are set with H = 10 cm and H = 30 cm.

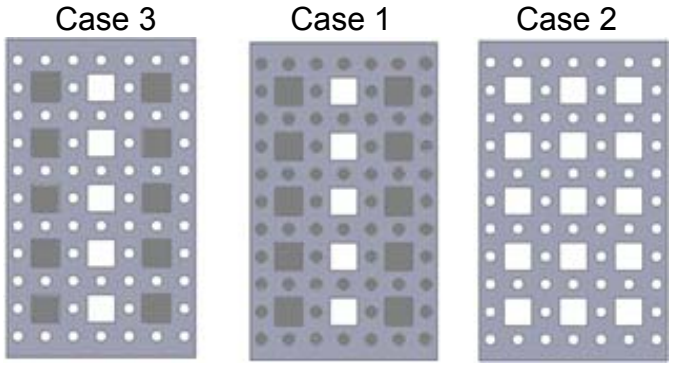

Fig. 4 Openings arrangement for backplane

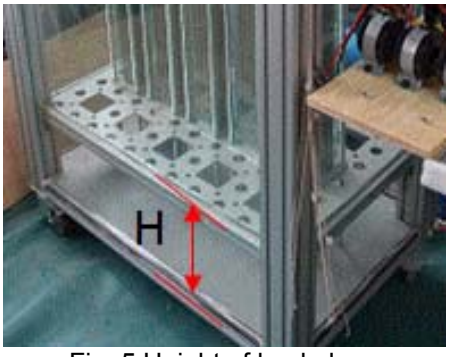

Fig. 5 Height of backplane

3. CFD SIMULATIONS FOR RESISTANCES OF AIR IN SCALED-DOWN SINGLE ASSEMBLY

3.1 Physical modeling

As shown in Fig. 6, it is an eighth of rod bundle model with 5 × 5 square-arrayed rods for CFD simulation. The rod diameter and length are 10 mm and 1.1 m, respectively. In order to reduce the time of calculation, the model of rod bundle can be simplified to eighth model and all section of rod bundle are unified. Fig. 7 shows the mesh structure on one of the section, and the mesh element is chosen the “Quad” type.

3.2 Mathematical modeling

The purpose of rod bundle simulation is mainly to obtain the viscous and inertial resistances coefficients with pressure drop of air. The air pressure drop of rod bundle is

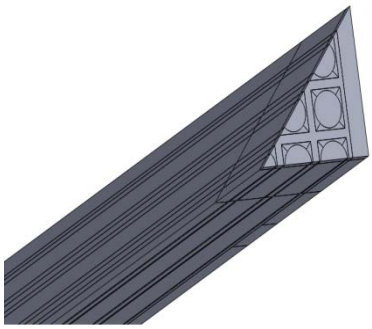

Fig. 6 CFD rod bundle modlel

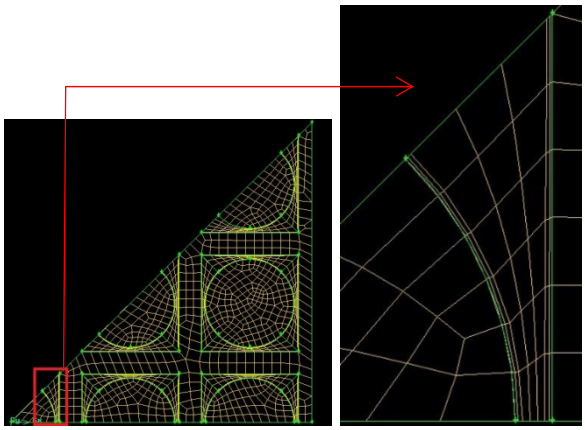

Fig. 7 Mesh structure

too difficult to measuring, so CFD simulations were employed to obtain it. The steady state problem was employed and the time ratio number was not a parameter to be concerned in present study.

The Darcy-Forchheimer-Brinkman model (Nield and Bejan 2006) is adopted to simulate the flow in porous medium, where both the inertia and viscosity effects are considered. The governing equations describing the conservations of mass, momentum and energy are listed as:

Continuity equation

$$\nabla \bullet (\rho \vec{V}) = 0 \tag{1}$$

Momentum equation in x-direction

$$\frac{1}{\varepsilon^2}(\vec{V} \cdot \nabla u) = -\frac{1}{\rho}\frac{\partial P}{\partial x} + \nu_m \cdot \nabla^2 u - \frac{\nu_f}{\alpha} u - \frac{C_2}{\sqrt{\alpha}} \left|\vec{V}\right| u \tag{2}$$

Momentum equation in y-direction

$$\frac{1}{\varepsilon^2}(\vec{V} \cdot \nabla \upsilon) = -\frac{1}{\rho}\frac{\partial P}{\partial y} + \nu_m \cdot \nabla^2 \upsilon - \frac{\nu_f}{\alpha} \upsilon - \frac{C_2}{\sqrt{\alpha}} \left|\vec{V}\right| \upsilon + g\beta(T - T_0) \tag{3}$$

Momentum equation in z-direction

$$\frac{1}{\varepsilon^2}(\vec{V}\cdot\nabla w) = -\frac{1}{\rho}\frac{\partial P}{\partial z} + \nu_m \cdot \nabla^2 w - \frac{\nu_f}{\alpha} w - \frac{C_2}{\sqrt{\alpha}}\left|\vec{V}\right| w \tag{4}$$

Energy equation

$$(\rho C_p)_f \cdot \vec{V} \cdot \nabla T = k_m \nabla^2 T + \varepsilon q_m \tag{5}$$

where ε is the porosity; ν_m and ν_f are the effective and fluid kinetic viscosity, respectively; α_f is the thermal diffusivity; β is thermal expansion; $\vec{V}$ is the velocity vector; u, υ and w represent the velocity components in x-, y-and z-directions; T is temperature and T_0 is environment temperature; k_m is the effective thermal conductivity of porous media, $k_m = (1-\varepsilon)k_s + \varepsilon k_f$, where k_s and k_f are the thermal conductivities of solid and fluid, respectively; q_m is the effective energy source term. Porous media are modeled by the addition of a momentum source term to the standard fluid flow equations. The source term is composed of two parts: a viscous loss term, and an inertial loss term. The source term is as follow

$$S = -(\frac{\mu}{\alpha}\upsilon + C_2 \frac{1}{2}\rho|V|\upsilon) \tag{6}$$

In which, S is the source term for momentum equation; μ is fluid viscosity; ρ is density; $|V|$ is the magnitude of velocity; α is the permeability and C_2 is the inertial resistance factor. This momentum sink contributes to the pressure gradient in the porous cell, creating a pressure drop that is proportional to the fluid velocity in the cell. The radiation transfer equation (Cheong and Song 1997, Tseng *et al*. 2007) can be written as

$$\Omega \cdot \nabla I(r\cdot\Omega) = -(a_{net} + \sigma_s) I(r,\Omega) + \kappa I_b(r) + \frac{\sigma_s}{4\pi} S(r,\Omega) \tag{7}$$

where a_{net} is the net absorption coefficient; σ_s is the scattering coefficient; $\kappa = a_{net} + \sigma_s$ is the extinction coefficient; Ω is the ordinate direction vector; $I(r,\Omega)$ is the intensity of radiation at location of r in a direction Ω; $I_b(r)$ is the black body intensity of radiation at a location r; $S(r,\Omega)$ is a source term.

4. RESULTS AND DISCUSSION

4.1 Pool model experiment

Fig. 8 presents the top view of a rod bundle and the front view of a pool model. As an example in the following discussion for Figs. 9-11, 3A3 represents rod bundle No. 3 with the rod located at A and thermal couple located at the height of 70 cm. In this

study, it aims to observe temperature distribution of the pool.

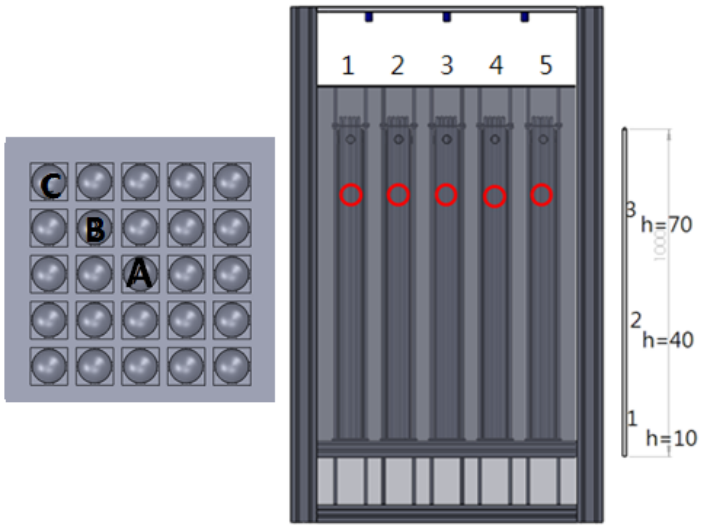

Fig. 8 Schematic illustration of rod location

As shown in Fig. 9, the temperature at the center of the pool is lower than other bundles particularly for higher power and at the location with greater height. This phenomenon does not happen around the bottom of the bundles. It is due to the effect of buoyancy driven heat transfer, air flows through the gap and converges center region of the pool and therefore less air will flow through the edge bundle such as No. 5. However, the rod at center of the specific bundle always has the higher temperature than other rods.

The influence of the backplane height is shown in Fig. 10, the temperature of a backplane at the height of 30 cm is lower than 10 cm about 10% to 20%. In the

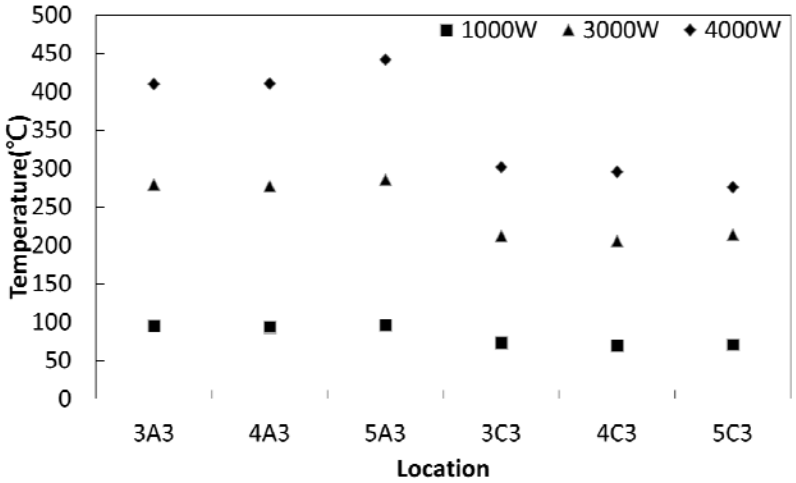

Fig. 9 Temperture distribution under various power

experiment of a backplane at 10 cm, the air accumulated at the bottom of pool model results in a poorer convection effect than the other one no matter which rod in the bundle.

The temperature influence on openings arrangement is shown in Fig. 11. Comparing the results of the three cases, temperature distribution of case 1 and case 3 are all about the same; case 2 has the lower temperature distribution. The purpose of case 1 was expected to guide the most air flow through the rod bundles, but the results of the experiment implies that Cases 1 and 3 cause greater flow resistance than that of Case 2. Because case 2 has more tunnels than other ones, it has the best convection to remove the heat.

4.2 Simulation for a pool with multiple fuel bundles

CFD simulation data of rod bundle is available in the form of pressure drop against velocity through the porous component, which can be extrapolated to determine the

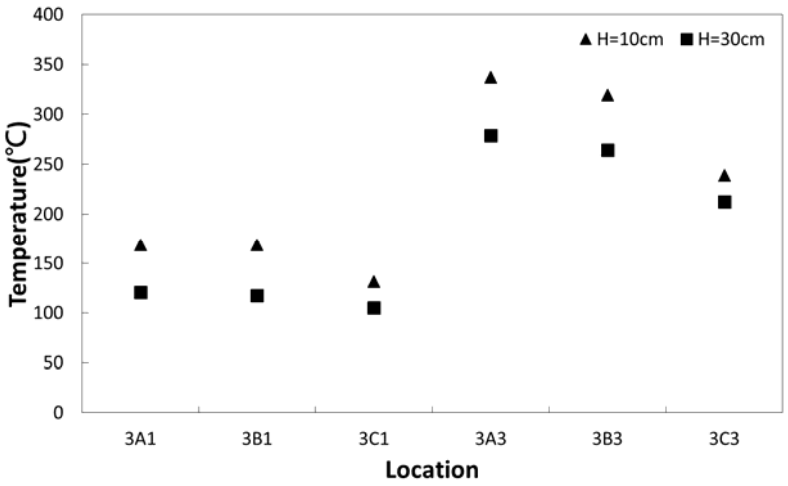

Fig. 10 Influence of backplan height

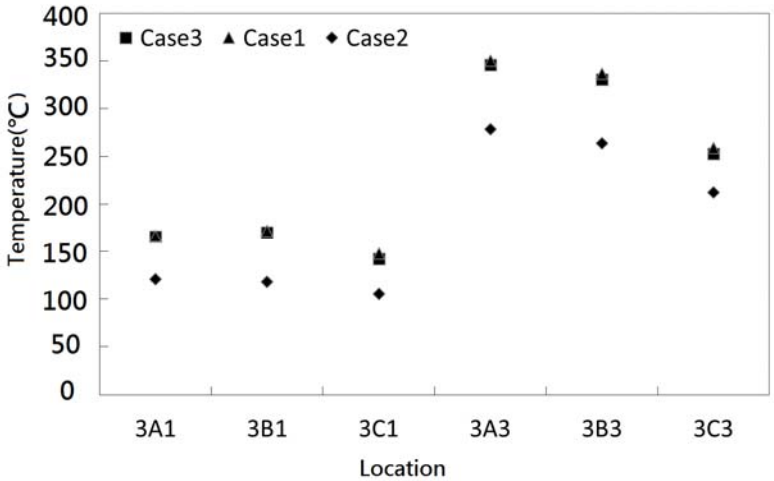

Fig. 11 Temperature distribution of three arrangements of openings

coefficients for the porous medium. As shown in Fig. 12, the relation between pressure drop and velocity can be obtained by interpolation method as follows

$$\Delta P = 1.75\upsilon^2 + 27.4\upsilon - 42.5 \tag{8}$$

Comparing Eq. (5) to Eq. (7) yields

$$1.75 = C_2 \frac{1}{2} P \tag{9}$$

$$27.4 = \frac{\mu}{\alpha} \tag{10}$$

In present study, ρ and μ of air are 1.18 kg/m^3 and 1.9 $\times$ 10^{-5} N-s/m^2, respectively and thus, the inertial resistance and the permeability are C_2 = -2.966 1/m and α = -6.94 $\times$ 10^{-8} m^2, respectively. As shown in Fig. 13, a quarter of the pool model was employed for CFD simulation because the phenomena are expected to be symmetrical in both x- and y-axis.

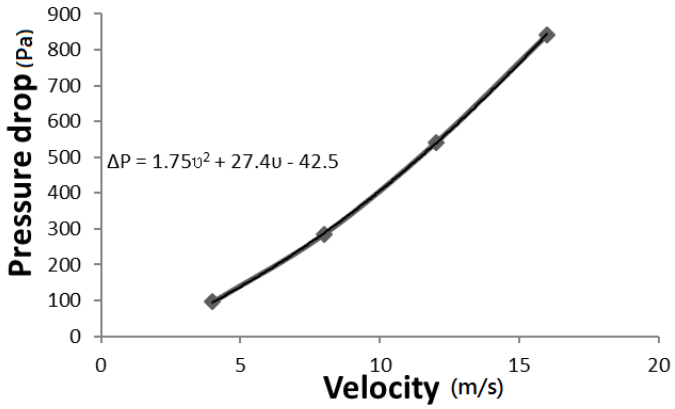

Fig. 12 ΔP-υ diagram

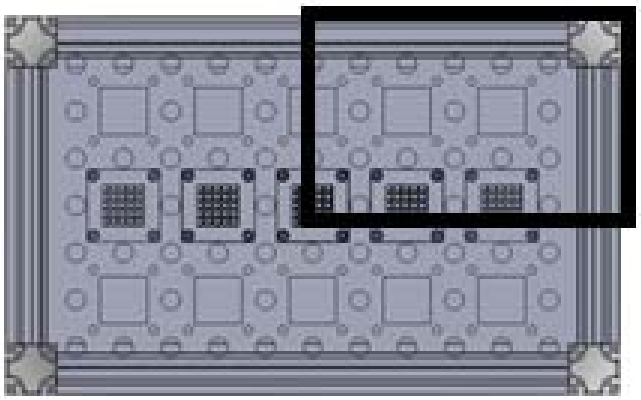

Fig. 13 A quarter of the pool model (top view)

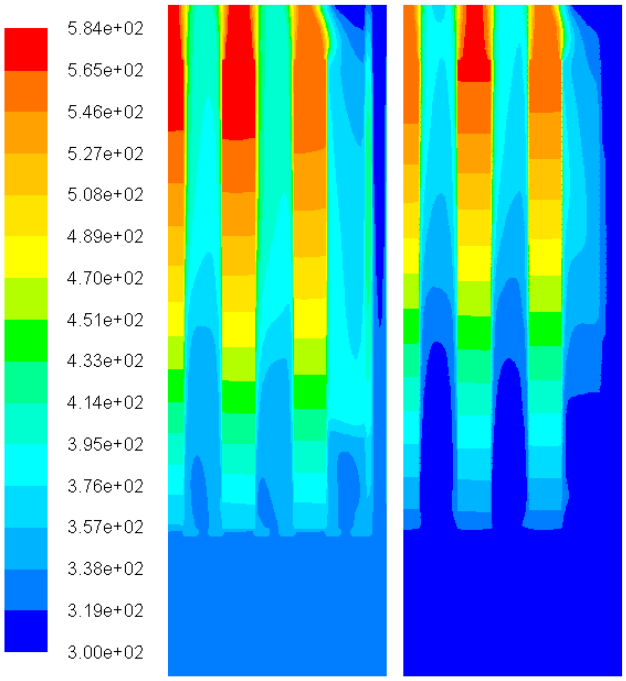

Fig. 14 Temperature distribution with radiation and non-radiation mode

Case 2 of the Fig. 4 has been implemented via CFD simulation. The temperature distributions of the pool model are shown in Fig. 14, in which the CFD simulations with radiation (left one) and without radiation (right one) mode are shown, respectively. The simulation results indicate that case including thermal radiation has a relatively higher average temperature than the right one (not including radiation). That is because the bottom of left one is heated by radiation. However, the right one has a peak value of

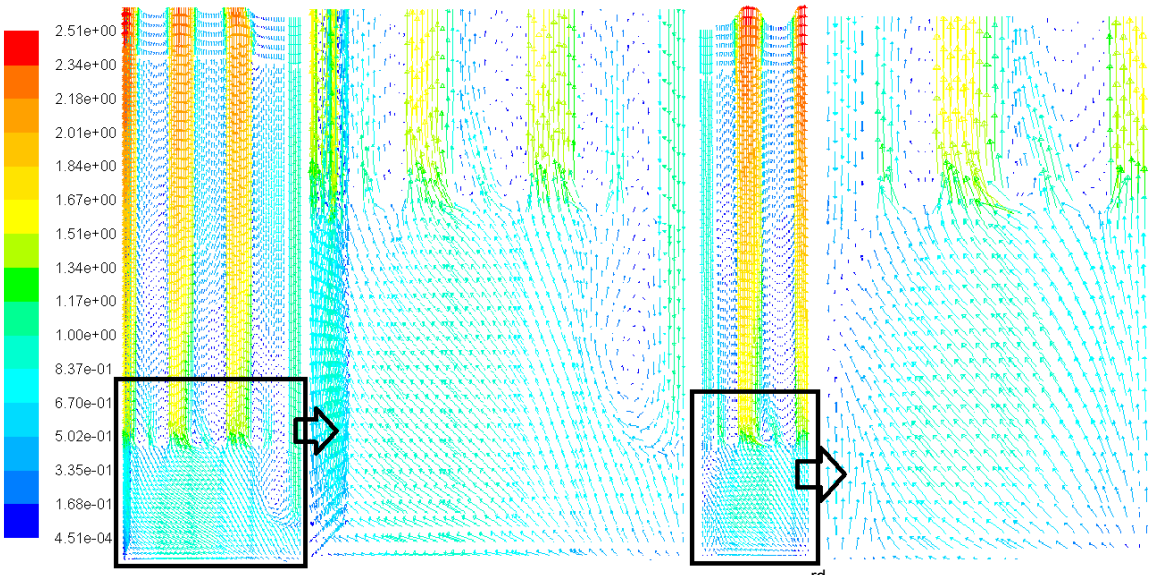

(a) front (b) left-side of 3rd bundle

Fig. 15 Velocity vector of the symmetrical cut-planes

temperature, which is higher than left one for about 6°C. Since thermal radiation exists in the real world and the above results indicate the difference, thermal radiation mode would be included in the following discussion.

The distributions of the velocity vector on the two symmetrical cut-planes are shown in Fig. 15; they are the front view and the view of left side, respectively. In the front view of pool model, because the effect of buoyancy force, the down-flow air from the gap will reflow to the rod bundles. The air in the rod bundles has a faster velocity, because the heating effect in the fuel region induces stronger buoyancy force. As shown in view of left side, air flows downward along the gap and mainly flows through the rod bundles. There is an interesting and important finding: the distribution of velocity and temperature in all the rod bundles are very uniform.

The comparisons between experiment and the CFD simulation are shown in Fig. 16. The parameters include the effect of backplane height and the effect of opening arrangement of the backplane. The temperature decreasing ratios are closed; the deviations of experiment and CFD simulation are between 6% and 20%. It can be seen that the behavior from CFD simulation is similar to that from experiment in present study. However, why the temperature values from measurement are much higher than that from numerical simulation? It is because the measured point is on the surface of the rod, which temperature is for sure higher than the porous like surface with fluid flow inside the porous region. Meanwhile, since there have many thermocouple wires above the experimental model, this somewhat enhances the flow resistance for air flow through the bundles in the central region of the pool.

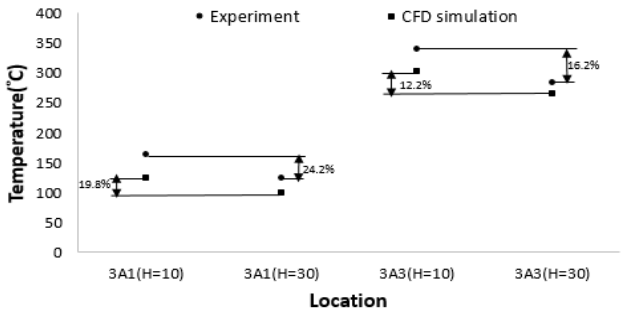

(a) Height of backplane

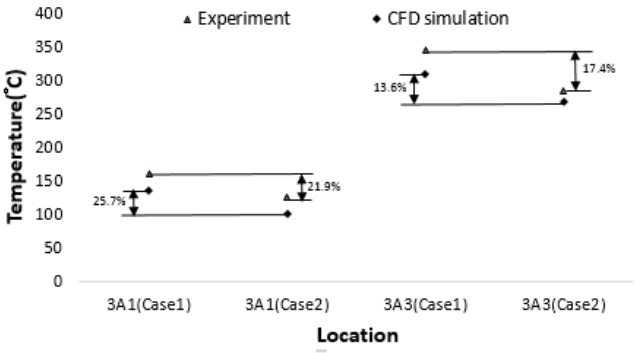

(b) Opening arrangement

Fig. 16 Comparison between experiment and CFD simulation

5. CONCLUSIONS

The radiation mode in CFD simulation must be considered under the possible temperature range and the concept of passive heat transfer is useful for present study. The viscous resistance and permeability have been determined based on the experiment data and detailed CFD simulations. Layout of the openings and the height of backplane are the important parameters to be investigated their influence in temperature of the pool and the fuel rods in present study. Buoyancy induced passive air convection could efficiently remove the decay heat for those fuels that have been moved out of the core for several years. The temperature distribution of the pool is truly influenced by the number of openings and their layout. Also, the temperature for the case with backplane height, H, of 30 cm is lower than the case of H = 10cm. The results indicate a faster air speed in the region of rod bundles than the neighbor spacing, and the fastest speed is occurred in the bundle No. 3. From above analysis, the CFD simulation is creditable in present study.

ACKNOWLEDGEMENTS

This research work has been supported by the National Science Council, Taiwan, R.O.C. under the grants of Contract No. NSC 101-3113-P-007-006 and NSC 102-3113-P-007-004.

REFERENCES

Arndt, B., Klaus, R. and Wasinger, K. (2003), “Advanced spent fuel storage pools?”, *Storage of spent fuel from power reactor*, 134-146.

Bodansky, D. (2000), *Nuclear energy*, Second edition, Oxford University Press, London, 253-258.

Biro, L. and Rodna, A. (2003), “A regulatory approach Implementation of Romanian NPP spent fuel management strategy”, *Storage of spent fuel from power reactor*, 55-66.

Cheong, K.B. and Song, T.H. (1997), “An alternative discrete ordinates method with interpolation and source differencing for two-dimensional radiative transfer problems”, *Numerical Heat Transfer A*, **32**, 107-125.

Conner, M.E., Baglietto, E. and Elmahdi, A.M. (2010), “CFD methodology and validation for single-phase flow in PWR fuel assemblies”, *Nuclear Engineering and Design*, **240**(9), 2088-2095.

Hung, T.C., Dhir, V.K., Pei, B.S., Chen, Y.S. and Tsai, F.P. (2013), “The development of a three-dimensional transient CFD model for predicting cooling ability of spent fuel pools”, *Applied Thermal Engineering*, **50**(1), 496-504.

Iqbal, M., Khan, J. and Mirza, S.M. (2006), “Design study of a modular dry storage facility for typical PWR spent fuel”, *Progress in Nuclear Energy*, **48**(6), 487-494.

Niyogi, K.K. and Tseng, C.W. (1983), “Thermal-hydraulics of a spent fuel pool”, *American Society of Mechanical Engineers pressure vessel and piping conference*,

Portland.
Nield, D.A. and Bejan, A. (1992), Convection in Porous Media, Springer, New York.
Navarro, M.A. and Santos, A.A.C. (2011), “Evaluation of a numeric procedure for flow simulation of a 5×5 PWR rod bundle with a mixing vane spacer”, *Progress in Nuclear Energy*, **53**(8), 1190-1196.
Steinberg N. and Afanasyev, A.A. (2003), “National policy in the area of spent fuel management in Ukraine: Current status and trends (prospective)”, *Storage of spent fuel from power reactor*, 76-84.
Smith, L.D. III, Conner, M.E., Liu, B., Dzodzo, M.B., Paramonov, D.V., Beasley, D.E., Langford H.M. and Holloway, M.V. (2002), “Benchmarking computational fluid dynamics for application to PWR fuel”, *Proceedings of the 10th International Conference on Nuclear Engineering*.
Tseng, Y.S., Pei, B.S. and Hung, T.C. (2007), “Effects of Thermal Radiation for Electronic Cooling on Modified PCB Geometry under Natural Convection”, Numerical *Heat Transfer*, *Part A*: *Applications*, **51**(2), 195-210.
U.S. Nuclear Regulatory Commission (1997), “Standard Review Plan for Dry Cask Storage Systems: Final Report”, NUREG-1536.